Dynamics and control of different aircraft formation structures

F. Giulietti
University of Bologna, Italy
G. Mengali
University of Pisa, Italy

ABSTRACT

The problem of aircraft formation dynamics and control is investigated from the viewpoint of formation architecture. Three different formation structures, leader-wingman, virtual leader and behavioural approaches are introduced. A comparative study is made using a unified approach through a suitable control law. The formation systems are analyzed on a quantitative basis and objective results are made available for the designer. The trade-off between system performance and complexity is indicated. A complete nonlinear simulation involving a flight-path change and a heading change manoeuvre is discussed. Results show the superiority of a behavioural approach to maintain close formations of vehicles.

NOMENCLATURE

≙	state matrix
≐	input matrix
C_{D_0}	zero-lift drag coefficient
C_D	drag coefficient
C_L	lift coefficient
D	drag force
K_V, K_ψ, K_γ	trajectory gain components
K_P	position gain matrix
K_T	trajectory gain matrix
$K_{P_{ij}}$	position gain components
L	lift force
P	Lapunov matrix
S	wing surface
T	engine thrust
V	airspeed
Δ	diagonal matrix
$\mathcal{R}$	rotation matrix
T_{VW}	local vertical to wind-axes rotation matrix
$\mathcal{T}_I$	inertial frame
$\mathcal{T}_V$	local vertical frame
$\mathcal{T}_W$	wind-axes frame
$\bar{q}$	dynamic pressure
g	gravitational acceleration
k	induced drag factor
m	aircraft mass
n	load factor
t	time
$\mathbf{r}_I$	inertial frame components
$\mathbf{V}$	velocity vector
δ, ξ	error vector components
d	relative distance vector
e	error vector
f, **g**, **h**	non-linear dynamics functions
r	position vector
u	input vector
x	state vector
$\boldsymbol{\omega}$	angular velocity components
Ω	cross-product matrix
ψ, γ, φ	heading, *i*ght-path and roll angles
ρ	air density
ω	angular velocity

Superscripts

-	desired
•	time derivative
T	transposed

Subscripts

$_C$	formation geometry center
$_i$	*i*_th aircraft
$_R$	reference
$_V$	virtual leader

Paper No. 2839. Manuscript received 28 April 2003, accepted 2 December 2003.

https://doi.org/10.1017/S0001924000151565 Published online by Cambridge University Press

1.0 INTRODUCTION

Aircraft formation control has become an active research area in recent years. In a manner similar to migratory birds, aircraft in a formation may experience a substantial drag reduction using the vortex upwash created by the leading aircraft[1]. This in turn implies a potential fuel reduction with significant benefits for military and commercial employments. Further important aspects motivating the growing attention towards this subject are as follows. It is believed that aircraft formation control will play a fundamental role in future aerospace scenarios, where unmanned air vehicles will be required to manoeuvre in swarms for surveillance, reconnaissance and rescue purposes in hostile environments[2]. Finally, autonomous formation flight systems are widely investigated due to their close connection to the aerial refuelling problem[3,4].

Most of the existing literature concerning the problem of aircraft formation control[5-9] and/or aerodynamic interference modelling[10-12], assumes a fixed formation structure. By contrast, in this paper the aircraft formation control is analyzed using different formation arrangements in order to establish a link between system performance and complexity. In particular, we concentrate on leader-wingman, virtual leader and behavioural approaches, that represent the three main structures reported in the literature[5-9, 13, 14].

In the leader-wingman structure the first aircraft in the formation is designated as the leader, whereas the remaining aircraft (wingmen) are viewed as followers. While the leader keeps a prescribed trajectory, the followers refer their position to the other aircraft in the formation. More precisely, they keep a fixed relative distance from the neighbouring aircraft and, in doing so, they form a chain. Although a rear aircraft usually exhibits a poorer response than its reference due to error propagations, for its simplicity the leader-wingman structure is widely employed in control and management of multiple vehicle formations[5-9].

In the virtual leader structure, instead, each aircraft receives the same information, that is, the trajectory of the virtual leader. This latter may be a real aircraft or, more commonly, an ideal point in the formation that aircraft must track. The advantage of a virtual leader structure is twofold:

1. all aircraft in the formation exhibit the same transient due to the absence of error propagations; and

2. the formation behaviour is prescribed by simply specifying the behaviour of the virtual leader. The disadvantage is that there is no explicit feedback to the formation. Indeed, each aircraft has no information about its distance from the followers and therefore may not be able to avoid collisions.

A quite different strategy is represented by the behavioural approach. In this structure, the control action of each aircraft is a weighted average of the control for each behaviour. In the context of aircraft formation control this idea has been first introduced by Anderson and Robbins[13]. Then, it has been further exploited by Giulietti *et al*[15] with the introduction of an imaginary point in the formation called the formation geometry centre (FGC). Each aircraft in the formation is required to maintain a prescribed distance from the FGC. The position of this point depends on the relative distances between all aircraft in the formation. This allows each aircraft to have the capability of sensing other vehicles' movements from the nominal position and to manoeuvre in order to re-establish the formation geometry. This characteristic is very similar to the natural behaviour of migratory birds[16]. The strength of this approach is that there is an explicit feedback to the formation so that problems of collision avoidance are easily taken into account. Another important advantage is that aircraft in a formation tend to cooperate with each other so that there are no points of failure in the structure. On the other hand, the behavioural approach is more complex than the others as it requires exchanging more information.

In this paper the above formation structures are analysed in a unified framework through a suitable control system architecture. The approach is inspired by that proposed by Beard *et al* for spacecraft formation control[17]. An important result is that in this way different formation systems are compared on a quantitative basis and objective conclusions are made available for the designer. In particular the trade-off between system performance and complexity is pointed out.

Although the stability of the formation dynamics is guaranteed only for the linearized model, all the simulations are performed in a nonlinear framework and without simplifying assumptions. From this viewpoint the paper represents an improvement over existing approaches where linear aircraft dynamics or formation planar models are employed[5,7].

2.0 FORMATION MODELLING

A three degrees-of-freedom point mass model is chosen to represent each aircraft in the formation. This simplified model, involving only the aircraft's slow states, is well suited for dealing with trajectory tracking problems and position keeping autopilots.

2.1 Reference frames

Aircraft dynamics are described with the aid of two right-hand reference frames: A local vertical frame $\mathcal{T}_V$ and a wind-axes frame $\mathcal{T}_W$. Both have their origins in the instantaneous position of the aircraft. It is assumed that $\mathcal{T}_V$ has axes parallel to an inertial frame $\mathcal{T}_I$. As usual, the axis x_W of $\mathcal{T}_W$ is directed along the velocity vector V and the axis z_W lies in the plane of symmetry of the aircraft.

The transformation between the vertical frame $\mathcal{T}_V$ and the wind-axes frame $\mathcal{T}_W$ is defined through the following rotation matrix:

$$\mathcal{T}_{WV} = \begin{bmatrix} \mathrm{Cos}\gamma\mathrm{Cos}\psi & \mathrm{Cos}\gamma\mathrm{Sin}\psi & \mathrm{Sin}\gamma \\ -\mathrm{Cos}\varphi\mathrm{Sin}\psi - \mathrm{Sin}\varphi\mathrm{Sin}\gamma\mathrm{Cos}\psi & \mathrm{Cos}\varphi\mathrm{Cos}\psi - \mathrm{Sin}\varphi\mathrm{Sin}\gamma\mathrm{Sin}\psi & \mathrm{Sin}\varphi\mathrm{Cos}\gamma \\ \mathrm{Sin}\varphi\mathrm{Sin}\psi - \mathrm{Cos}\varphi\mathrm{Sin}\gamma\mathrm{Cos}\psi & -\mathrm{Sin}\varphi\mathrm{Cos}\psi - \mathrm{Cos}\varphi\mathrm{Sin}\gamma\mathrm{Sin}\psi & \mathrm{Cos}\varphi\mathrm{Cos}\gamma \end{bmatrix} \quad . . (1)$$

where ψ, γ and φ correspond to aircraft heading, flight-path and roll angles. For convenience we choose the flight-path angle γ with the sign reversed with respect to the usual notations. This means, for instance, that the aircraft rate of climb is given by $-V\mathrm{Sin}\gamma$, where V is the aircraft velocity. Also, we use the following notation: If $\mathbf{w}$ is an arbitrary vector, its components are transformed from $\mathcal{T}_W$ to $\mathcal{T}_V$ through the relation

$$[\boldsymbol{w}]_W = \mathcal{T}_{WV}[\boldsymbol{w}]_V \quad . . (2)$$

2.2 Aircraft equations of motion

The equations of motion of i-th aircraft in the formation are

$$\dot{V}_i = \frac{T_i - D_i}{m_i} + g\,\mathrm{Sin}\gamma_i \quad . . (4)$$

$$\dot{\psi}_i = \frac{g}{V_i}\frac{n_i\mathrm{Sin}\varphi_i}{\mathrm{Cos}\gamma_i} \quad . . (5)$$

$$\dot{\gamma}_i = -\frac{g}{V_i}\left(n_i\mathrm{Cos}\varphi_i - \mathrm{Cos}\gamma_i\right) \quad . . (6)$$

where

$$n_i \triangleq \frac{L_i}{m_i g} \quad . . (7)$$

is the load factor, L_i and D_i are lift and drag forces, T_i is the engine thrust, m_i is the aircraft mass and g is the gravitational acceleration. Using the aircraft drag polar, the drag coefficient C_{D_i} is given by

https://doi.org/10.1017/S0001924000151565 Published online by Cambridge University Press

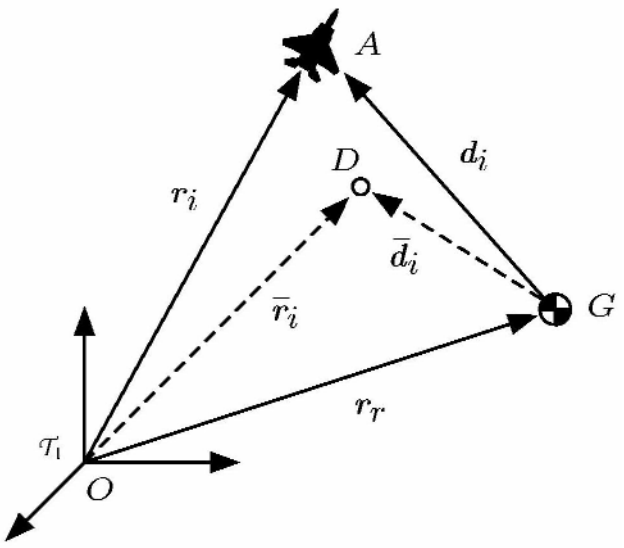


Figure 1. Definition of geometric quantities with actual (*A*) and desired (*D*) positions of *i*-th aircraft.

$$C_{D_i} = C_{D_{0_i}} + k_i C_{L_i}^2 \quad \ldots (7)$$

where C_{L_i} is the lift coefficient, C_{D0_i} is the zero-lift drag coefficient and k_i is the induced drag factor. The aerodynamic drag force is computed as:

$$D_i = \bar{q}_i S_i C_{D_{0_i}} + k_i \frac{(n_i m_i g)^2}{\bar{q}_i S_i} \quad \ldots (8)$$

where $\bar{q}_i = \frac{1}{2}\rho V_i^2$ is the dynamic pressure, ρ is the atmospheric density and S_i is the wing surface. Variations in aerodynamic forces due to the trailing vortices for each aircraft have been computed with a distributed horse-shoe vortex technique[1,18]. Such effects are implicitly contained in the expressions of force coefficients.

Introducing the state vector $\mathbf{x_i} \triangleq [V_i, \psi_i, \gamma_i]^T$ and the input vector $\mathbf{u_i} \triangleq [T_i, n_i, \varphi_i]^T$, the aircraft equations of motion (3)-(5) can be written in standard form as:

$$\mathbf{x_i} = \mathbf{f_i}(\mathbf{x_i}, \mathbf{u_i})$$

2.3 Position kinematics

One of the main issues in a formation flight control system is to provide each aircraft with the ability to maintain a prescribed distance from a certain reference point *G*. This may coincide with the formation leader (either real or virtual), a neighboring aircraft, or a certain point within the aircraft formation.

To establish a suitable mathematical model, assume that $\mathbf{r_i}$ and $\mathbf{r_r}$ are the positions of *i*-th aircraft and reference point with respect to the origin *O* of the inertial frame. Let be the relative actual position between *G* and the *i*-th aircraft, while the corresponding desired position is represented by an overbarred symbol. Also assume that an orthogonal frame $\mathcal{T}_{Wr}$ is 'attached' to the reference point *G* whose orientation is defined through Euler angles $\bar{\varphi}$, $\bar{\gamma}$, $\bar{\psi}$ and let $\bar{\mathbf{V}}$ be the velocity of *G*. With reference to Fig. 1 the following relations are obtained:

$$\mathbf{r_r} + \mathbf{d_i} = \mathbf{r_i} \quad \ldots (10)$$

and

$$\mathbf{r_r} + \bar{\mathbf{d}}_\mathbf{i} = \bar{\mathbf{r}}_\mathbf{i} \quad \ldots (11)$$

from which we get:

$$\mathbf{d_i} - \bar{\mathbf{d}}_\mathbf{i} = \mathbf{r_i} - \bar{\mathbf{r}}_\mathbf{i} \quad \ldots (12)$$

Taking the derivative of (12) with respect to the $\mathcal{T}_{Wi}$ frame yields:

$$\dot{\mathbf{d}}_\mathbf{i} - \dot{\bar{\mathbf{d}}}_\mathbf{i} + \boldsymbol{\omega}_\mathbf{i} \times (\mathbf{d_i} - \bar{\mathbf{d}}_\mathbf{i}) = \mathbf{V_i} - \bar{\mathbf{V}}_\mathbf{i} \quad \ldots (13)$$

where ω_i is the angular velocity of the wind-axes frame $\mathcal{T}_{Wi}$ relative to the local vertical frame $\mathcal{T}_V$. To stress the fact that vectors are evaluated in the wind-axes frame of the *i*-th aircraft, Equation (13) is written as:

$$\left[\dot{\mathbf{d}}_\mathbf{i}\right]_{\mathbf{W_i}} = \left[\mathbf{V_i}\right]_{\mathbf{W_i}} - \left[\bar{\mathbf{V}}_\mathbf{i}\right]_{\mathbf{W_i}} - \Omega_i \left[\mathbf{d_i} - \bar{\mathbf{d}}_\mathbf{i}\right]_{\mathbf{W_i}} + \left[\dot{\bar{\mathbf{d}}}_\mathbf{i}\right]_{\mathbf{W_i}} \quad \ldots (14)$$

where

$$\Omega_i \triangleq \begin{bmatrix} \mathbf{0} & -\mathbf{R_i} & \mathbf{Q_i} \\ \mathbf{R_i} & \mathbf{0} & -\mathbf{P_i} \\ -\mathbf{Q_i} & \mathbf{P_i} & \mathbf{0} \end{bmatrix} \quad \ldots (15)$$

is the cross-product matrix and $[\boldsymbol{\omega}_i]_{W_i} \triangleq [P_i, Q_i, R_i]^T$. Note that:

$$P_i = \dot{\varphi}_i + \dot{\psi}_i \mathrm{Sin}\gamma_i \quad \ldots (16)$$

$$Q_i = -\dot{\gamma}_i \mathrm{Cos}\varphi_i + \dot{\psi}_i \mathrm{Cos}\gamma_i \mathrm{Sin}\varphi_i \quad \ldots (17)$$

$$R_i = \dot{\psi}_i \mathrm{Cos}\gamma_i \mathrm{Cos}\varphi_i + \dot{\gamma}_i \mathrm{Sin}\varphi_i \quad \ldots (18)$$

Assume that the desired orientation of the *i*-th aircraft coincides with that of the frame $\mathcal{T}_{Wr}$ and that the corresponding desired velocity $\bar{\mathbf{V}}_\mathbf{i}$ equals the velocity of the reference point $\bar{\mathbf{V}}$. Defining the rotation matrices:

$$\mathcal{T}_{W_iV} \triangleq \mathcal{T}_{WV}(\varphi_i, \gamma_i, \psi_i) \quad \ldots (19)$$

and

$$\mathcal{T}_{W_rV} \triangleq \mathcal{T}_{WV}(\bar{\varphi}, \bar{\gamma}, \bar{\psi}) \quad \ldots (20)$$

where $\mathcal{T}_{WV}$ is given by Equation (1), one has:

$$\left[\bar{\mathbf{V}}\right]_{W_i} = \mathcal{T}_{W_iV}\left[\bar{\mathbf{V}}\right]_V \quad \ldots (21)$$

and

$$\left[\bar{\mathbf{V}}\right]_{W_r} = \mathcal{T}_{W_rV}\left[\bar{\mathbf{V}}\right]_V \quad \ldots (22)$$

Using (21) and (22) gives the desired velocity vector in the reference frame $\mathcal{T}_{Wi}$:

$$\left[\bar{\mathbf{V}}\right]_{W_r} = \mathbb{R}\left[\bar{\mathbf{V}}\right]_{W_r} \quad \ldots (23)$$

where

$$\mathbb{R} \triangleq \mathcal{T}_{W_iV}\mathcal{T}_{W_rV}^T \quad \ldots (24)$$

and

$$\left[\bar{\mathbf{V}}\right]_{W_r} = \left[\bar{\mathbf{V}}, 0, 0\right]^T \quad \ldots (25)$$

Substituting (23) into (14) and dropping for simplicity the square brakets, the position dynamics of the *i*-th aircraft relative to the reference point in the frame $\mathcal{T}_{Wi}$ are:

$$\dot{\boldsymbol{d}}_i = \mathbf{V}_i - \mathbb{R}\bar{\mathbf{V}} - \Omega_i(\boldsymbol{d}_i - \bar{\boldsymbol{d}}_i) + \dot{\bar{\boldsymbol{d}}}_i \quad \ldots (26)$$

https://doi.org/10.1017/S0001924000151565 Published online by Cambridge University Press

Note that, if we introduce the state vector of the reference system $\bar{\boldsymbol{x}} \triangleq \left[\bar{V}, \bar{\psi}, \bar{\gamma}\right]^T$, the position dynamics of the *i*-th aircraft with respect to the reference point may also be written in compact form as:

$$\dot{\mathbf{d}}_\mathbf{i} = \mathbf{g}(\mathbf{x_i}, \bar{\mathbf{x}}, \mathbf{d_i}, \bar{\mathbf{d}}_\mathbf{i}, \mathbf{u_i}) \quad \ldots (27)$$

3.0 FORMATION CONTROL

This section outlines the formation control system design. It is assumed that standard autopilot loops have been closed around each aircraft in the formation. Our aim is to define a formation control law that is able to fulfil simultaneously two different tasks: (*i*). trajectory tracking and (*ii*) position keeping. In the following, a suitable control vector in the form

$$\mathbf{u_i} = \mathbf{h}(\mathbf{x_i}, \bar{\mathbf{x}}, \mathbf{d_i}, \bar{\mathbf{d}}_\mathbf{i}) \quad \ldots (28)$$

is used to guarantee that each aircraft in the formation has the following dynamics:

$$\dot{\mathbf{x}}_\mathbf{i} = -K_x(\mathbf{x_i} - \bar{\mathbf{x}}) - K_d(\mathbf{d_i} - \bar{\mathbf{d}}_\mathbf{i}) \quad \ldots (29)$$

where

$$\mathbf{K_x} = \begin{bmatrix} K_V & 0 & 0 \\ 0 & K_\psi & 0 \\ 0 & 0 & K_\gamma \end{bmatrix} \quad \ldots (30)$$

and

$$\mathbf{K_d} = \begin{bmatrix} K_{d_x} & 0 & 0 \\ 0 & K_{d_y} & 0 \\ 0 & 0 & K_{d_z} \end{bmatrix} \quad \ldots (31)$$

are positive definite gain matrices.

To get the required control efforts a dynamic inversion approach is employed. More precisely, the commanded rates in Equation (29) are set equal to the actual rates in Equations (3)-(5) and a solution is found for thrust, bank angle, and load factor. From flight-path and heading equations we obtain respectively:

$$n_i \mathrm{Cos}\varphi_i = \frac{V_i}{g}\left[K_\gamma(\gamma_i - \bar{\gamma}) - K_{d_z}(d_{z_i} - \bar{d}_{z_i})\right] + \mathrm{Cos}\gamma_i \triangleq \quad \ldots (32)$$

and

$$n_i \mathrm{Sin}\varphi_i = \frac{V_i}{g}\left[-K_\psi(\psi_i - \bar{\psi}) - K_{d_y}(d_{y_i} - \bar{d}_{y_i})\right]\mathrm{Cos}\gamma_i \triangleq \quad \ldots (33)$$

Note that the ratio between Equation (33) and Equation (32) provides the required bank angle command:

$$\varphi_i = \mathrm{Arctan}\left(\frac{f_2}{f_1}\right) \quad \ldots (34)$$

while the sum of the squares of Equations (33) and (32) gives the required load factor:

$$n_i = \sqrt{f_1^2 + f_2^2} \quad \ldots (35)$$

The thrust command is obtained from the following equation:

$$-K_V(V_i - \bar{V}) - K_{d_x}(d_{x_i} - \bar{d}_{x_i}) = \frac{T_i - D_i}{m_i} - g\mathrm{Sin}\gamma_i \quad \ldots (36)$$

Solving for the thrust produces:

$$T_i = D_i - m_i K_V(V_i - \bar{V}) - m_i K_{d_x}(d_{x_i} - \bar{d}_{x_i}) - m_i g\mathrm{Sin}\gamma_i \quad \ldots (37)$$

where D_i is computed through Equation (8). Clearly, Equations (34), (35) and (37) are equivalent to (28). To summarise, the closed loop dynamics of the *i*-th aircraft are given by (see Equations (9), (27) and (28)):

$$\begin{aligned} \dot{d}_i &= g\left(x_i, \bar{x}, d_i, \bar{d}_i, u_i\right) \\ \dot{x}_i &= f\left(x_i, u_i\right) \\ u_i &= h\left(x_i, \bar{x}, d_i, \bar{d}_i\right) \end{aligned} \quad \ldots (38)$$

The form of the closed loop dynamics (38) general model is quite general and encompasses different formation structures. Some of the most significant structures are now described.

4.0 FORMATION STRUCTURES

4.1 Leader-wingman structure

The leader-wingman is a commonly employed structure for control and management of multiple-vehicle formation. The leader aircraft directs the whole formation while keeping a prescribed trajectory. The other aircraft (wingmen) have to maintain a given distance from the neighboring ones. The mathematical model for the generic aircraft in the the leader-wingman structure is:

$$\begin{aligned} \dot{d}_i &= g\left(x_i, x_{i\text{-}1}, d_i, \bar{d}_i, u_i\right) \\ \dot{x}_i &= f\left(x_i, u_i\right) \\ u_i &= h\left(x_i, x_{i\text{-}1}, d_i, \bar{d}_i\right) \end{aligned} \quad \ldots (39)$$

where the subscripts *i*-1 indicates the neighboring aircraft.

4.2 Virtual leader structure

The virtual leader structure can be viewed as a variation of the leader-wingman structure. Each aircraft is expected to follow an imaginary point in the formation (the virtual leader), while keeping a prescribed relative distance from it. The main difference with respect to the leader-wingman structure consists in that each aircraft receives the same trajectory information i.e., the virtual leader position. A mathematical model for this system is given by:

$$\begin{aligned} \dot{d}_i &= g\left(x_i, x_{VL}, d_i, \bar{d}_i, u_i\right) \\ \dot{x}_i &= f\left(x_i, u_i\right) \\ u_i &= h\left(x_i, x_{VL}, d_i, \bar{d}_i\right) \end{aligned} \quad \ldots (40)$$

where the subscript *VL* indicates the virtual leader.

4.3 Behavioural approach (formation geometry centre structure)

The behavioural approach is a quite different strategy with respect to those described previously. In this case each aircraft is required to keep a relative distance from an imaginary point (the formation geometry centre) whose dynamics depends on all the aircraft positions in the formation. This allows each aircraft to 'perceive' the movement of the other vehicles from the nominal position. In the presence of disturbances, for instance, if an aircraft loses its position, the others sense a change in the formation structure. As a result, they depart momentarily from the prescribed trajectory, manoeuvring so

https://doi.org/10.1017/S0001924000151565 Published online by Cambridge University Press

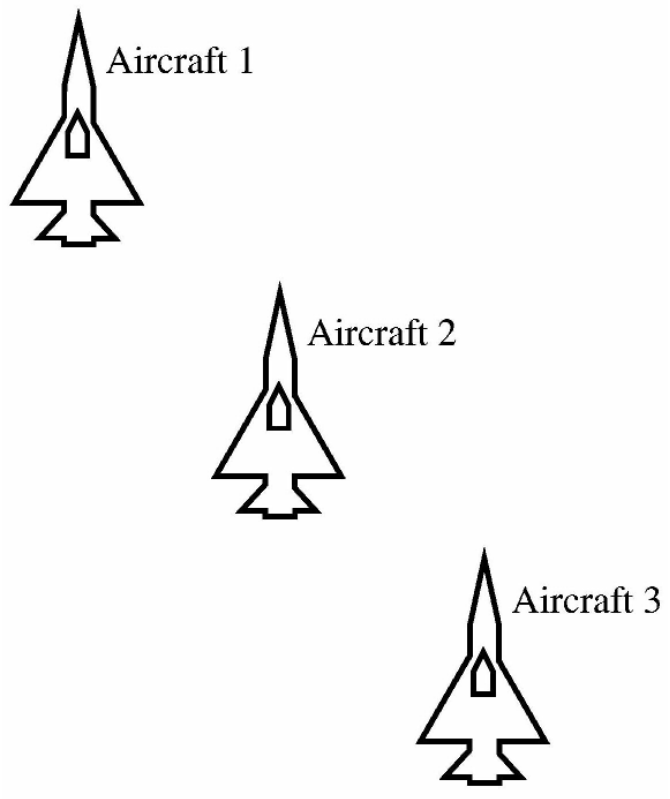


Figure 2. Formation arrangement.

as to reconstitute the formation geometry. The mathematical model for the generic aircraft in a n_a-aircraft formation is given by:

$$\begin{aligned}\dot{d}_i &= g\left(x_i, x_G, d_i, \bar{d}_i, u_i\right)\\ \dot{x}_i &= f\left(x_i, u_i\right)\\ u_i &= h\left(x_i, x_G, d_i, \bar{d}_i\right)\end{aligned} \quad \ldots (41)$$

where $\boldsymbol{x}_{\mathbf{G}} = \left[\mathbf{V}_{\mathbf{G}}, \psi_{\mathbf{G}}, \gamma_{\mathbf{G}}\right]^{\mathbf{T}}$ is the state vector of the formation geometry centre. It is assumed that:

$$\begin{aligned}V_G &= \sqrt{\dot{x}_G^2 + \dot{y}_G^2 + \dot{z}_G^2}\\ \psi_G &= \mathrm{Arctan}\left(\dot{y}_G / \dot{x}_G\right)\\ \gamma_G &= \mathrm{Arcsin}\left(\dot{z}_G / V_G\right)\end{aligned} \quad \ldots (42)$$

where, by definition

$$\begin{bmatrix}\dot{x}_G\\ \dot{y}_G\\ \dot{z}_G\end{bmatrix} \triangleq \frac{1}{n_a}\sum_{i=1}^{n_a}\begin{bmatrix}V_i \mathrm{Cos}\gamma_i \mathrm{Cos}\psi_i\\ V_i \mathrm{Cos}\gamma_i \mathrm{Sin}\psi_i\\ V_i \mathrm{Sin}\gamma_i\end{bmatrix} \quad \ldots (43)$$

Equation (43) shows that all aircraft contribute to establishing the geometry centre position.

Note that the equations of motion for the three formation structures have the same form as expressed in Equations (38) general model. This allows us to treat the stability problem in an unified framework. This subject is discussed in the next section.

5.0 FORMATION STABILITY

We turn our attention to the closed loop dynamics (38) general model aiming to investigate its stability properties. With the aid of Equations (26) and (29) the mathematical model may be rewritten as

$$\dot{d}_i - \dot{\bar{d}}_i = -\Omega_i\left(d_i - \bar{d}_i\right) + V_i - \mathbb{R}\bar{V} \quad \ldots (44)$$

$$\dot{x}_i - \dot{\bar{x}}_i = -K_d\left(\mathbf{d}_\mathbf{i} - \bar{\mathbf{d}}_\mathbf{i}\right) - K_x\left(x_i - \bar{x}\right) - \dot{\bar{x}} \quad \ldots (45)$$

Equations (44) to (45) are useful for simulations, but in order to prove the system stability, a linearised version of Equation (44) is employed. More precisely, if 0 represents the trim value and $\Delta(\cdot)$ the generic first order variation, the linear approximation of Equation (44) is given by

$$\Delta\dot{d}_i - \Delta\dot{\bar{d}}_i = Y\left(\Delta x_i - \Delta\bar{x}\right) \quad \ldots (46)$$

where it has been assumed that $\Omega_0 = 0_{3\times 3}$ and

$$\mathbf{V} \triangleq \begin{pmatrix}1 & 0 & 0\\ 0 & \mathrm{V}_0 & 0\\ 0 & 0 & \mathrm{V}_0\end{pmatrix} \quad \ldots (47)$$

is a positive definite diagonal matrix. Correspondingly, Equations (44)-(45) become

$$\begin{aligned}\dot{\boldsymbol{\delta}}_i &= Y\boldsymbol{\xi}_i\\ \dot{\boldsymbol{\xi}}_i &= -K_d\boldsymbol{\delta}_i - K_x\boldsymbol{\xi}_i - \dot{\bar{\boldsymbol{x}}}\end{aligned} \quad \ldots (48)$$

where $\boldsymbol{\delta}_i \triangleq \Delta\boldsymbol{d}_i - \Delta\bar{\boldsymbol{d}}_i$, $\boldsymbol{\xi}_i \triangleq \Delta\boldsymbol{x}_i - \Delta\bar{\boldsymbol{x}}$. The stability of the linearised system complete system around the trim condition is guaranteed by the following theorem.

Theorem 1. Define the error vector $\dot{\boldsymbol{e}}_i \triangleq \left[\boldsymbol{\delta}_i^T, \xi_i^T\right]^T$ and suppose $\dot{\bar{\boldsymbol{x}}} \in L_2[0,\infty) \cap L_\infty[0,\infty)$. Then, $\|\boldsymbol{e}_i\| \to 0$ as $t \to \infty$.

Proof See Appendix.

6.0 SIMULATION RESULTS

The nonlinear Equations (38) have been employed in comparing the properties of the three formation structures. Each formation is made of three F-16 aircraft models and the general arrangement is shown in Fig. 2. The aircraft parameters are summarised in Table 1.

The simulations deal with a trajectory tracking task. Starting with a velocity of 200ms^{-1} and a height of 6,000m each aircraft is required to perform a flight-path change and a heading change manoeuvre. The commanded trajectory is represented in Fig. 3 and is described as follows. First, a ramp-like flight-path change of –6° is applied over $\tau \in [25,30]s$. The value $\gamma = -6°$ is then kept until $t = 40$s when a +6° ramp-like flight-path change is produced over $\tau \in [40,45]s$. Second, a ramp-like heading change of –60° is generated over $\tau \in [70,100]s$. Figures 4-9 show the simulation results.

Figure 4 illustrates the z-axis distance error of the aircraft in a leader-wingman structure during the flight-path change manoeuvre. It points out the performance limits of such a structure due to the error propagations along the vehicle chain. Clearly the front aircraft has a better response than the rear aircraft. Figures 5-7 compare the three formation structures by showing the y-axis distance error for each aircraft during the heading change manoeuvre. Note that the behavioural and the virtual leader structures have the same characteristics for all the three aircraft in the formation, while, once again, the leader-wingman structure has a degrading performance from the

https://doi.org/10.1017/S0001924000151565 Published online by Cambridge University Press

Table 1
Simulation data

Parameter	Value
Wing area, S	27·87m^2
Wing span, b	9·14m
Aspect ratio, AR	3
Lift curve slope, $C_{L\alpha}$	5·3rad^{-1}
Zero-Lift drag coefficient, C_{D0}	0·015
Induced drag factor, k	0·1118
Mass, m	11,336kg
Velocity gain, K_V	5s^{-1}
Flight-path gain, K_γ	3s^{-1}
Heading gain, K_ψ	3s^{-1}
x-axis distance gain, K_x	0·5s^{-2}
y-axis distance gain, K_y	0·03m^{-1}s^{-1}
z-axis distance gain, K_z	s0·03m^{-1}s^{-1}

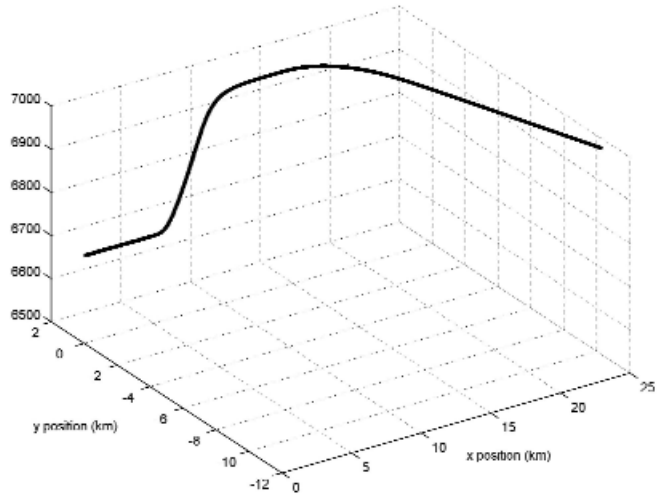


Figure 3. Desired trajectory.

front to the rear of the formation.

It is interesting to see what happens when a system failure occurs. Suppose for instance that the central aircraft (Aircraft 2 in Fig. 2) cannot keep the prescribed position in the formation. In our example this happens when its feedback with the distance measurement fails, or $K_d = 0$. The simulations are shown in Figs 8, 9 and 10.

Figure 8 illustrates the leader-wingman case. As anticipated, the Aircraft 2 cannot keep its distance relative to Aircraft 1 and, in fact, the position error shows up after the heading change manoeuvre and propagates in the formation. Although Aircraft 3 has no steady-state relative error, it does have an absolute position error because it looks at Aircraft 2.

Let us now concentrate on Fig. 9 dealing with a virtual structure. The time histories look similar to those of the leader-wingman case but an important difference exists. As in the previous case Aircraft 2 cannot keep its position and accumulates a position error after the heading change manoeuvre. However, now Aircraft 3 (which now looks at the virtual leader trajectory) has no absolute position error. This is an important point because it says that each aircraft exhibits the same transient. At the same time it also implies that a virtual structure formation does not possess a real formation feedback and, therefore, a protection against collisions cannot be guaranteed.

As Fig. 10 shows, the situation in the behavioural structure case is quite different. Here the capability exists of sensing each aircraft

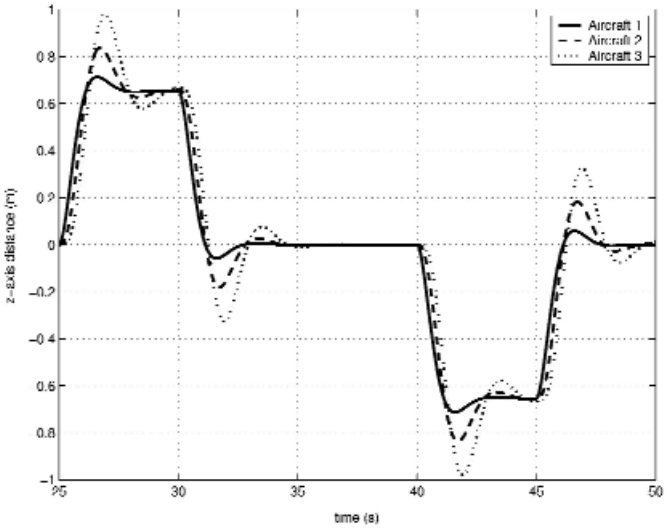


Figure 4. Leader-wingman structure: z-axis distances during flight-path change manoeuvre.

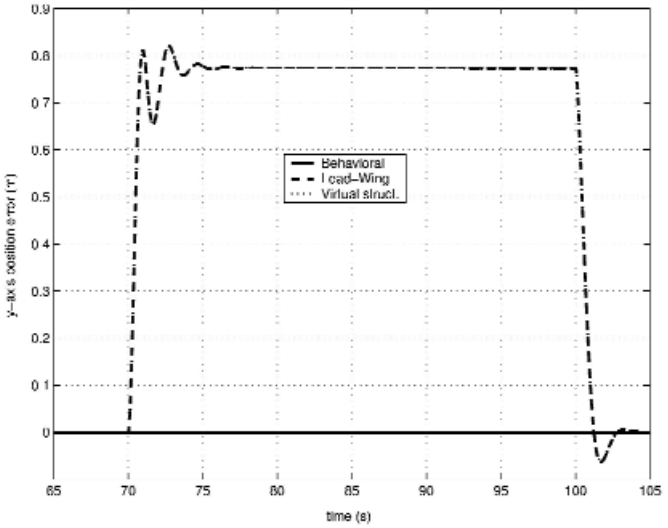


Figure 5. Aircraft 1: y-axis position error within the three structures.

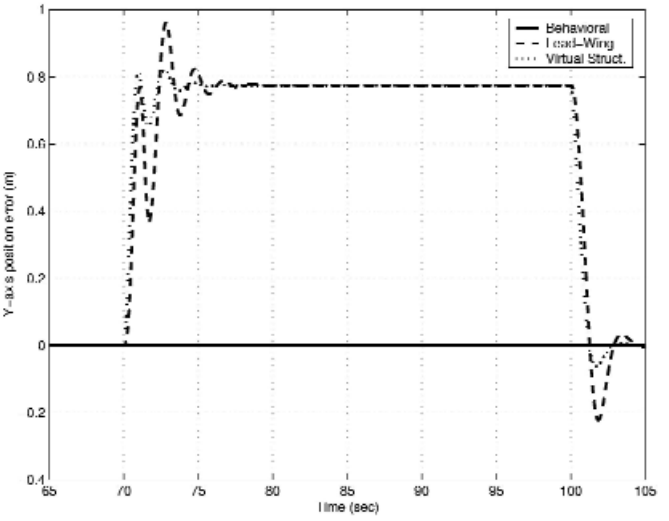


Figure 6. Aircraft 2: y-axis position error within the three structures.

https://doi.org/10.1017/S0001924000151565 Published online by Cambridge University Press

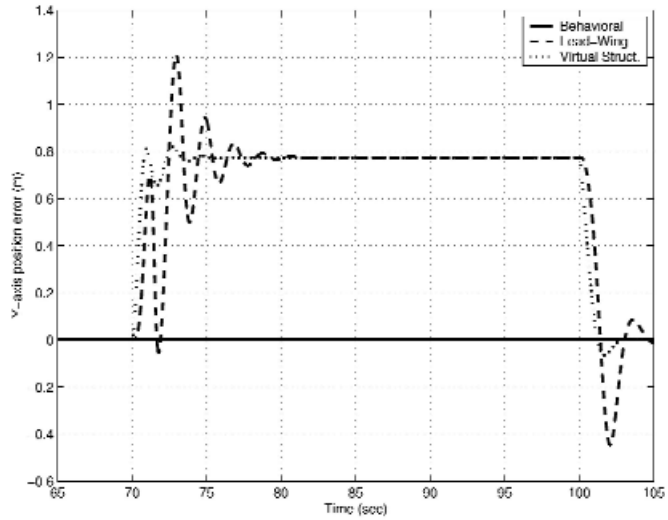


Figure 7. Aircraft 3: *y*-axis position error within the three structures.

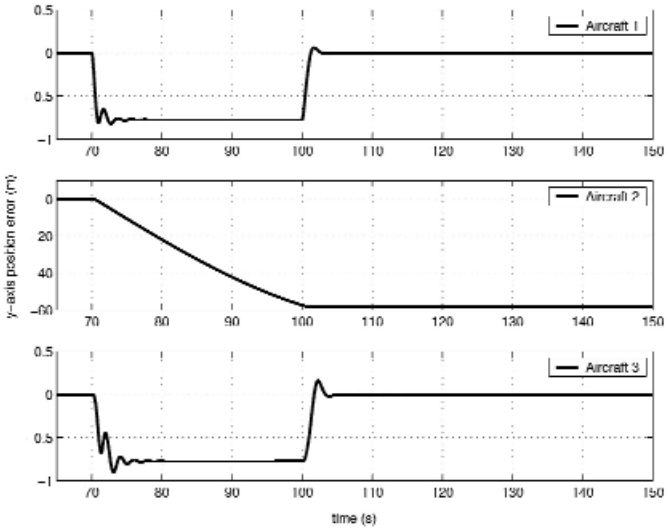


Figure 8. Leader-wingman structure formation: position error along *y*-axis.

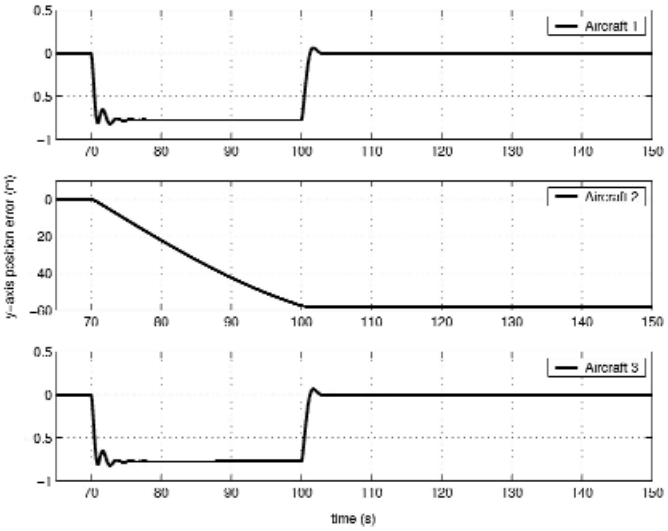


Figure 9. Virtual structure formation: position error along *y*-axis.

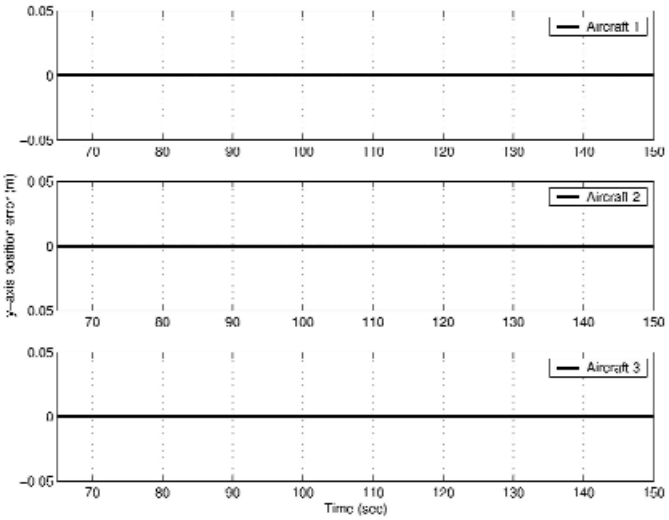


Figure 10: Behavioural structure formation : position error along *y*-axis.

movement from the prescribed position. As a result, when Aircraft 2 takes a wrong position, Aircraft 1 and 3 manoeuvre so as to remove the position error with respect to their common reference (the FGC point). Therefore the behavioural approach is the best way to obtaining close vehicle formations and allows both adequate trajectory tracking and geometry formation keeping. On the other hand it needs more information because each aircraft has to know all the aircraft states.

7.0 CONCLUSIONS

The problem of aircraft formation dynamics and control has been investigated from the viewpoint of the formation architecture. Three different formation structures have been compared in an unified manner. A suitable control law has also been described and analyzed. Our approach is physically intuitive, simple to handle and is guaranteed to be stable at least in the linearised case. An important contribution of the paper is that different formation structures may be analyzed on a quantitative basis and objective results are made available for the designer. In this way the trade-off between system performance and complexity may be fully exploited. A nonlinear simulation of a flight-path change and a heading change manoeuvre has been illustrated. The results show the superiority of the behavioural approach for it guarantees both trajectory tracking and formation keeping with no propagation errors. Exploiting the formation geometry centre concept, it also avoids collisions because each aircraft senses the others' movements. On the other hand, the behavioural approach is more complex because each aircraft needs knowledge of all the other state vectors.

APPENDIX: PROOF OF THEOREM 5

Consider the closed loop dynamics (48) and define the error vector $\dot{\boldsymbol{e}}_i \triangleq \left[\boldsymbol{\delta}_i^T, \xi_i^T\right]^T$. One has:

$$\dot{\boldsymbol{e}}_i = A\boldsymbol{e}_i - B\ddot{\boldsymbol{x}}$$

where Y is given by Equation (47) and

https://doi.org/10.1017/S0001924000151565 Published online by Cambridge University Press

$$\mathbf{A} = \begin{bmatrix} \mathbf{0} & \mathbf{Y} \\ -\mathbf{K}_d & -\mathbf{K}_x \end{bmatrix} \quad ; \quad \mathbf{B} = \begin{bmatrix} \mathbf{0} \\ \mathbf{I} \end{bmatrix} \qquad \ldots (50)$$

Recall that K_x and K_d are both diagonal and positive definite matrices (see Equations (30) to (31)). We first prove the stability of

$$\dot{\boldsymbol{e}}_i = A\boldsymbol{e}_i \qquad \ldots (51)$$

To this end we introduce the Lyapunov candidate $\mathcal{V}(\boldsymbol{e}_i) = \frac{1}{2}\boldsymbol{e}_i^T P \boldsymbol{e}_i$, where

$$\mathbf{P} = \begin{bmatrix} \mathbf{I} & \varepsilon\mathbf{I} \\ \varepsilon\mathbf{I} & \mathbf{Y}\left(\mathbf{K}_d\right)^{-1} \end{bmatrix} \qquad \ldots (52)$$

and $\varepsilon > 0$ is a scalar. Note that P is positive definite for small values of ε since

$$\mathbf{P} = \begin{bmatrix} \mathbf{I} & \varepsilon\mathbf{K}_d\mathbf{Y}^{-1} \\ 0 & \mathbf{I} \end{bmatrix} \begin{bmatrix} \mathbf{I} - \varepsilon^2\mathbf{K}_d\mathbf{Y}^{-1} & 0 \\ 0 & \mathbf{Y}\left(\mathbf{K}_d\right)^{-1} \end{bmatrix} \begin{bmatrix} \mathbf{I} & 0 \\ \varepsilon\mathbf{K}_d\mathbf{Y}^{-1} & \mathbf{I} \end{bmatrix} \qquad \ldots (53)$$

and $(K_d)^{-1} = \text{diag}(1/K_{d_x}, 1/K_{d_y}, 1/K_d)$ and $(Y)^{-1}$. Differentiating $\mathcal{V}$ we get:

$$\dot{\mathcal{V}} = -\boldsymbol{e}_i^T Q \boldsymbol{e}_i \qquad \ldots (54)$$

where

$$Q = -\frac{1}{2}(A^T P + PA) \qquad \ldots (55)$$

We claim that Q is positive definite. In fact, as $Q = Q^T$, Q may be partitioned as (see Ref. 19)

$$\mathbf{Q} = \begin{bmatrix} \mathbf{Q}_{11} & \mathbf{Q}_{12} \\ \mathbf{Q}_{12}^T & \mathbf{Q}_{22} \end{bmatrix} = \begin{bmatrix} \mathbf{I} & \mathbf{Q}_{12}\mathbf{Q}_{22}^{-1} \\ \mathbf{0} & \mathbf{I} \end{bmatrix} \begin{bmatrix} \mathbf{Q}_{11} - \mathbf{Q}_{12}\mathbf{Q}_{22}^{-1}\mathbf{Q}_{12}^T & \mathbf{0} \\ \mathbf{0} & \mathbf{Q}_{22} \end{bmatrix} \begin{bmatrix} \mathbf{I} & \mathbf{0} \\ \mathbf{Q}_{22}^{-1}\mathbf{Q}_{12}^T & \mathbf{I} \end{bmatrix} \qquad \ldots (56)$$

It is easily checked that $\left(\mathbf{Q}_{22}^{-1}\right)^T = \mathbf{Q}_{22}^{-1}$ because $\mathbf{Q}_{22} = \mathbf{Y}\left[\mathbf{K}_x\left(\mathbf{K}_d\right)^{-1}\right.$ is a diagonal matrix. Accordingly, Equation (56) is in the form $Q = NMT^T$ and is Q positive definite if and only if M is positive definite. Now,

$$\begin{bmatrix} \mathbf{e}\mathbf{K}_d + \varepsilon^2\mathbf{F} & \mathbf{0} \\ \mathbf{0} & \mathbf{Y}\left[\mathbf{K}_x\left(\mathbf{K}_d\right)^{-1} - \varepsilon\mathbf{I}\right] \end{bmatrix} \qquad \ldots (57)$$

where F is a diagonal matrix whose entries contain the entries of K_d, K_x and Y. For instance, it may be checked that

$$F(1,1) = \frac{1}{4}\frac{K_V^2 K_{d_x}}{\varepsilon K_{d_x} - K_V} \qquad \ldots (58)$$

and so on. It is concluded that M (and hence Q) is positive definite for sufficiently small ε. This means that $\mathcal{V}$ is a Lyapunov function, the system (51) is stable, and $\|\boldsymbol{e}_i\| \to 0$ as $t \to \infty$. Returning now to Equation (49), we see that it involves the extra term $\ddot{\boldsymbol{x}} \in L_2[0,\infty) \cap L_\infty[0,\infty)$. However this term does not affect the stability of Equation (49) as a consequence of Lemma 1 in Ref. 17.

REFERENCES

1. BREUKENBERG, M. and HUMMEL, D. Aerodynamics, performance and control of airplanes in formation flight, 1990, 17th ICAS Congress proceedings, September 1990, **2**, pp 1777-1794.
2. SINGH, S.N., CHANDLER, P., SCHUMACHER, C., BANDA, S. and PACHTER, M. Nonlinear adaptive close formation control of unmanned aerial vehicles, *Dynamics and Control*, April 2000, **10**, (2), pp 179-194.
3. BLOY, A.W., WEST, M.G., LEA, K.A. and JOUMA'A, M. Lateral aserodynamic interference between tanker and receiver in air-to-air refuelling, *J Aircr*, 1993, **30**, pp 705-710.
4. BLOY, A.W. and JOUMA'A, M. Lateral and directional stability control in air-to-air refuelling, *J Aerospace Eng*, 1995, **209**, pp 299-305.
5. PACHTER, M., D'AZZO, J.J. and PROUD, A.W. Tight formation flight control, *J Guidance, Control and Dynamics*, March-April 2001, **24**, (2), pp 246-254.
6. PROUD, A.W., PACHTER, M. and D'AZZO, J.J. Close formation flight control, 1999, AIAA Guidance, Navigation and Control Conference, AIAA Paper 99-4207, Portland, OR, August 1999.
7. PACHTER, M., D'AZZO, J.J. and DARGAN, J. Automatic formation flight control, *J Guidance, Control and Dynamics*, November-December 1994, **17**, (6), pp 1380-1383.
8. BUZOGANY, L.E., PACHTER, M. and D'AZZO, J.J. Automated control of aircraft in formation flight, 1993, AIAA Guidance, Navigation and Control Conference, Monterey, CA, August 1993, pp 1349-1370.
9. STANKOVIC, S.S., STANOJEVIC, M. and SILIAK, D.D. Decentralised overlapping control of a platoon of vehicles, 2000, IEEE Transaction on Control Systems Technology, **8**, (5), September 2000, pp 816-832.
10. GINGRAS, D.R. Experimental investigation of a multi-aircraft formation, 1999, AIAA Applied Aerodynamics Conference, AIAA Paper 99-3143, Norfolk, VA, June 1999.
11. GINGRAS, D.R., PLAYER, J.L., and BLAKE, W.B. Static and dynamic wind tunnel testing of air vehicles in close proximity, 2001, AIAA Atmospheric Flight Mechanics Conference and Exhibit, AIAA Paper 2001-4137, Montreal, Canada, August 2001.
12. NELSON, R.C. and JUMPER, E.J. Aircraft wake vortices and their effect on following aircraft, 2001, AIAA Atmospheric Flight Mechanics Conference and Exhibit, AIAA Paper 2001-4073, Montreal, Canada, August 2001.
13. ANDERSON, M.R. and ROBBINS, A.C. Formation flight as a cooperative game, 1998, AIAA Guidance, Navigation and Control Conference, AIAA Paper 98-4124, Philadelphia, PA, August 1998.
14. GIULIETTI, F., POLLINI, L. and INNOCENTI, M. Autonomous formation flight, *IEEE Control Systems Magazine*, December 2000, **20**, (6), pp 34-44.
15. GIULIETTI, F., POLLINI, L. and INNOCENTI, M. Formation flight control: a behavioral approach, 2001, AIAA Guidance, Navigation and Control Conference, AIAA Paper 2001-4239, Montreal, Canada, August 2001.
16. VAN TYNE, J. and BERGESR, A.J. *Fundamentals of Ornithology*, John Wiley, New York, 1976.
17. BEARD, R.W., LAWTON, J. and HADAEGH, F.Y. A coordination architecture for spacecraft formation control, IEEE Transactions on Control Systems Technology, November 2001, **9**, (6), pp 777-790.
18. GIULIETTI, F., NAPOLITANO, M., CAPETTA, R. and INNOCENTI, M. Detailed modeling of multiple aircraft within a close formation flight, 2002, AIAA Atmospheric Flight Mechanics Conference and Exhibit, AIAA Paper 2002-4404, Monterey, CA, August 2002.
19. ZHOU, K., DOYLE, J.C. and GLOVER, K. *Robust and Optimal Control*, 1996, pp 37-38, Prentice Hall, Upper Saddle River, NJ.

https://doi.org/10.1017/S0001924000151565 Published online by Cambridge University Press